Computers in Biology and Medicine 124 (2020) 103930

Contents lists available at ScienceDirect

Computers in Biology and Medicine

journal homepage: www.elsevier.com/locate/compbiomed

Accelerating Chan–Vese model with cross-modality guided contrast enhancement for liver segmentation

Nitin Satpute [a,*], Juan Gómez-Luna [b], Joaquín Olivares [a]

[a] Department of Electronic and Computer Engineering, Universidad de Córdoba, Spain
[b] Department of Computer Science, ETH Zurich, Switzerland

ARTICLE INFO

Keywords:
GPU
Contrast enhancement
Image segmentation
Persistence
Chan–Vese

ABSTRACT

Accurate and fast liver segmentation remains a challenging and important task for clinicians. Segmentation algorithms are slow and inaccurate due to noise and low quality images in computed tomography (CT) abdominal scans. Chan–Vese is an active contour based powerful and flexible method for image segmentation due to superior noise robustness. However, it is quite slow due to time-consuming partial differential equations, especially for large medical datasets. This can pose a problem for a real-time implementation of liver segmentation and hence, an efficient parallel implementation is highly desirable. Another important aspect is the contrast of CT liver images. Liver slices are sometimes very low in contrast which reduces the overall quality of liver segmentation. Hence, we implement cross-modality guided liver contrast enhancement as a pre-processing step to liver segmentation. GPU implementation of Chan–Vese improves average speedup by 99.811 (± 7.65) times and 14.647 (± 1.155) times with and without enhancement respectively in comparison with the CPU. Average dice, sensitivity and accuracy of liver segmentation are 0.656, 0.816 and 0.822 respectively on the original liver images and 0.877, 0.964 and 0.956 respectively on the enhanced liver images improving the overall quality of liver segmentation.

1. Introduction

Image segmentation is a popular research topic in medical imaging; as it has a number of applications, such as tissue detection [1], segmentation [2–5], reconstruction [6], registration [6,7], etc. There are many methods proposed for image segmentation, such as region growing [8], thresholding [9], gradient approach [3], contour methods [10,11], etc. They can be classified into edge or region based image segmentation methods. These methods can be further categorized based on histogram, spatial information of the image, convergence of active contours, etc [4,12]. The active contour models are essential when the edge of the region of interest in the image is indistinct and diffused [4,13]. The computed tomography (CT) scans sometimes provide poor quality images with indistinguishable liver boundaries which complicates the task of liver segmentation for clinicians for the treatment of patients.

The Chan–Vese algorithm is developed on active contour models using a level set approach [4,14]. This operates on the initial contours, average intensity values inside and outside the curve and optimizes the energy based on the level set approach [15,16]. The algorithm works on the principle of the energy minimization problem which relies on calculus and partial differential equations [17,18]. It is one of the most influential and effective methods in order to optimize the Mumford–Shah function which includes energy terms defined in image and contour space [12,19,20]. Chan–Vese is flexible and robust at segmenting the CT liver image, which is difficult to segment using classical segmentation techniques [10,21].

The study proposes a high performance Chan–Vese approach for liver segmentation by avoiding intermediate memory transfers between the CPU and GPU. However, the Chan–Vese approach alone is not sufficient for accurate liver segmentation as it can result in many false positives, lowering the sensitivity and accuracy [22,23] and degrading the quality of liver segmentation. Hence, we employ an enhancement module before the Chan–Vese approach for segmentation. This module provides the cross-modality guided liver contrast enhancement. This works on the target and guided image. We consider the CT liver image as the target image and the image from magnetic resonance (MR) imaging as the guided image. The cross-modality approach generates the histogram of target CT scan similar to guided MR image [24,25]. The proposed parallel approach results in fast and accurate liver segmentation.

Our goal is to develop a fast parallel Chan–Vese approach for liver segmentation with and without liver contrast enhancement. The GPU

* Corresponding author.
E-mail address: el2sasan@uco.es (N. Satpute).

https://doi.org/10.1016/j.compbiomed.2020.103930
Received 20 May 2020; Received in revised form 22 July 2020; Accepted 22 July 2020
Available online 29 July 2020

implementation is faster compared to the CPU and the liver contrast enhancement improves the quality of liver segmentation by reducing the false positives and increasing the sensitivity, dice score and accuracy of the segmentation. The average dice score, sensitivity and accuracy of the liver segmentation are 0.877 ± 0.036, 0.964 ± 0.037 and 0.956 ± 0.022 respectively after liver contrast enhancement improving the quality of segmentation. GPU implementation of the Chan–Vese segmentation algorithm improves the average speedup by 99.811 ± 7.65 times and 14.647 ± 1.155 times with and without enhancement in comparison to the CPU.

The rest of the paper is structured as follows. Section 2 briefs the background and motivation with respect to the Chan–Vese approach for image segmentation. Section 3 explains the flow of the Chan–Vese approach and its parallel implementation on the GPU both with and without liver contrast enhancement. Performance evaluation based on the quality of liver segmentation and the speedup is analyzed in Section 4. Section 5 summarizes the results and main conclusions of the paper.

2. Background and motivation

Image segmentation plays a vital role in medical image analysis. There are many methods developed for image segmentation [8]. Other researchers have investigated active contour models for image segmentation [4,14,17,18]. We explain the background and motivation behind active contours and the benefits of Chan–Vese approach for image segmentation.

Scientists have explored the snake model for segmentation. Snakes are defined as a set of points around a contour [26–28]. The contour can be initialized inside the object forcing the snake to expand outside. This is the Balloon Force algorithm [29,30]. The energy of the snake based model which provides a high quality segmentation can be defined as follows. Total energy of curve C

$$E(C) = E_{internal}(C) + E_{external}(C) \tag{1}$$

Eq. (1) expresses the total energy where the curve repeatedly evolves to minimize energy E. $E_{internal}(C)$ and $E_{external}(C)$ depend on the shape of the snake curve and image intensities respectively.

$$E_{internal}(C) = \int_0^1 w_1\|c'(s)\|^2 + w_2\|c''(s)\|^2 ds \tag{2}$$

Eq. (2) expresses the internal energy. Low c' means the curve is not too stretchy and it keeps the points on the curve together. Low c'' implies the curve is not too bendy i.e. it is smooth and keeps the points on the curve from oscillating.

$$F(s) = -[(\frac{\partial I(X(s),Y(s))}{\partial X})^2 + (\frac{\partial I(X(s),Y(s))}{\partial Y})^2] \tag{3}$$

$$E_{external}(C) = \int_0^1 -\|\nabla I(c(s))\|^2 ds = \int_0^1 F(s) ds \tag{4}$$

If there is no edge then $\nabla I(c(s)) = 0$ and $F(s) = 0$ (from Eqs. (3) and (4)). If there is a thick edge then $\|\nabla I(c(s))\|$ is large and $F(s)$ is more negative. It implies that the $E_{external}(C)$ is lowered. The aim is to minimize E(C) from Eq. (1). However, the contour never sees the distant strong edges and the snake gets hung up due to many small noises in the image [26,27,29,30]. Hence researchers devised a solution called a gradient vector flow (GVF). Instead of using an image gradient, they created a new vector field over the image plane [31,32]. The mathematical representation of GVF [33,34] is given by the following equations.

$$GVF1 = [(\frac{\partial V_x}{\partial x})^2 + (\frac{\partial V_x}{\partial y})^2 + (\frac{\partial V_y}{\partial x})^2 + (\frac{\partial V_y}{\partial y})^2] \tag{5}$$

$$GVF2 = \|\nabla e\|^2\|V - \nabla e\|^2 \tag{6}$$

$$cost\_GVF = \iint \mu(GVF1) + GVF2 \quad dxdy \tag{7}$$

GVF has two components defining smoothness (GVF1 from Eq. (5)) and edge map (GVF2 from Eq. (6)) as shown in Eq. (7). If ∇e is high then the gradient is also high and V follows the edge gradient faithfully. If ∇e is low then the gradient is also low and V becomes as smooth as possible. μ is a tuning parameter to define the scaling of smoothness in comparison to the edge map. GVF2 from Eq. (6) defines the characteristic of the image where ∇e is a magnitude of the edge map and $(V - \nabla e)$ shows similarity between V and ∇e. If the region has a thick edge (high ∇e) then $(V - \nabla e)$ should be low which implies V is pushed towards ∇e.

Nevertheless, there are problems with both the snake and GVF models [26,28,32]. They require the number of points and point distribution to be monitored. Snakes as defined can never wrap around multiple objects at once. They cannot determine the inner boundary of the region of interest. Hence researchers devised another solution called level sets [17,18,35]. The shape-intensity prior level set proposed by Wang et al. [35] contains the atlases which are weighted in the selected training datasets by calculating the similarities between the atlases and the test image to dynamically generate a subject-specific probabilistic atlas for the test image.

The idea of level sets is derived from fluid dynamics. Instead of parameterizing the curve using a set of ordered points, discretize the image plane (x,y) and define a function f(x,y). $f(x,y) > 0$ implies the pixels are inside the curve and $f(x,y) < 0$ describes the pixels are outside the curve [12,15].

In the absence of strong edges, we can use a region based formulation which is a Chan–Vese approach for segmentation [4,12,20].

$$SD_{inside} = \int_{inside} (I(x,y) - \mu_{inside})^2 dxdy \tag{8}$$

SD_{inside} from Eq. (8) denotes the standard deviation of pixels inside the curve.

$$SD_{outside} = \int_{outside} (I(x,y) - \mu_{outside})^2 dxdy \tag{9}$$

$SD_{outside}$ from Eq. (9) denotes the standard deviation of pixels outside the curve.

$$SD_{total} = \lambda_1 * SD_{inside} + \lambda_2 * SD_{outside} + \lambda_3 * LC + \lambda_4 * AUC \tag{10}$$

SD_{total} from Eq. (10) represents the Chan–Vese algorithm where LC is the length of the curve, AUC is the area under the curve and $\lambda_1 > 0, \lambda_2 > 0, \lambda_3 \geq 0, \lambda_4 \geq 0$ are fixed parameters [15,20]. The algorithm maximizes the difference in standard deviations of pixel distributions between inside and outside the curve.

The default value of λ is 0.1. It describes the relative weighting of curve smoothness. However, after experimentation, the authors found the following values (in Eq. (10)) suitable for convergence and accurate liver segmentation. The weight parameter of the term inside the level set is $\lambda_1 = 0.2$. The weight parameter of the term outside the level set is $\lambda_2 = 0.2$. The weight parameter of the length term is $\lambda_3 = 0.04 * width(image) * height(image)$ and $\lambda_4 = 0.0002 * width(image) * height(image)$ is the weight parameter of the area term.

In the next section, we discuss the CPU and GPU implementation of the Chan–Vese approach for liver segmentation.

3. Methodology

In this section, we discuss the proposed methodology based on the Chan–Vese approach and the impact of cross-modality guided contrast enhancement on liver segmentation. The sequential and parallel implementations of the Chan–Vese approach with and without liver contrast enhancement are explained in the following sections.

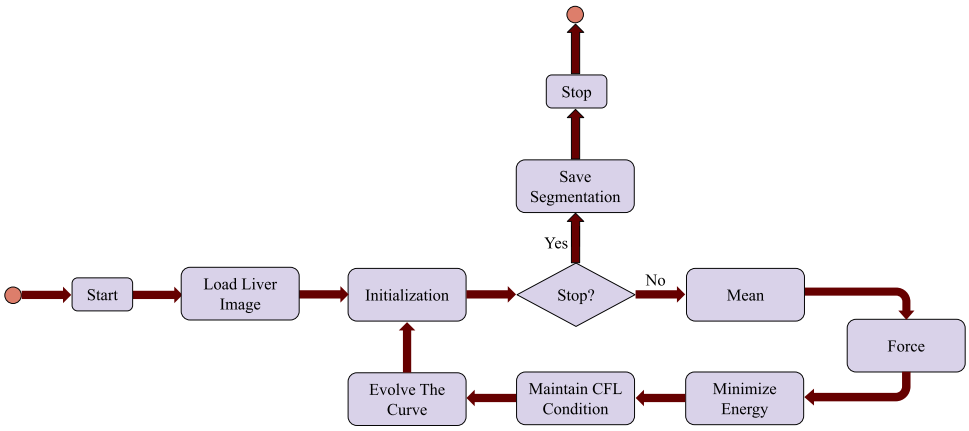

Fig. 1. CPU implementation of Chan–Vese.

3.1. CPU implementation of Chan–Vese

In this section, we discuss the flowchart for CPU implementation of the Chan–Vese approach for liver segmentation. The flowchart in Fig. 1 represents the Chan–Vese approach for liver segmentation.

- Initialization: The aim of this step is to create a mask or the initial contour in order to generate a signed distance function (SDF) [14,20]. This consists of two regions i.e. the liver as the foreground and the non-liver region as the background. The mask should be similar to the liver area in order to increase the sensitivity of segmentation and reduce the computation time.
- Stopping Criteria: This step detects if the process of liver segmentation is complete or not. If the process is complete then the segmented image is stored and the process of liver segmentation stops, otherwise the model calculates the mean of the interior and exterior regions with respect to the initial mask.
- Mean: This step includes the computation of the SDF as the first step. This is computed from the initial mask on the liver using Euclidean distance. In this work, we choose ϕ as an image with real values in order to choose distances from the curve so that the distance function (SDF) is positive inside the curve and negative outside. However, the computation of the SDF is time-consuming. Hence we apply a narrow band approach to reduce the computation time by restricting the computation to a band of grid points near the level set (or mask). The SDF helps to find the average value of pixels inside and outside the curve [14,19].
- Force: The calculation of the average value of the pixels inside and outside the curve is essential to compute the force from the Chan–Vese energy Eq. (11).

$$E = SD_{in} + SD_{out} = \int_{in} (I(x,y) - \mu_{in})^2 dxdy + \int_{out} (I(x,y) - \mu_{out})^2 dxdy \quad (11)$$

Force is computed from the image using the average value of the pixels inside and outside the curve as shown in Eq. (12).

$$F = \nabla E = (I(x,y) - \mu_{in})^2 + (I(x,y) - \mu_{out})^2 \quad (12)$$

Then the curvature is calculated using the kappa equation [12,15] and the central difference approximation scheme is applied to approximate the derivatives of SDF with respect to x and y.

- Minimize Energy: The gradient descent algorithm helps to minimize the energy given by Eq. (11). The curve is updated by the calculation of the SDF after a small time interval and is approximated by the first-order Taylor expansion.
- Maintain CFL Condition: The Courant, Friedrichs, Lewy (CFL) [14,15,19] condition is necessary for convergence while solving the partial differential equations in order to maintain the accuracy of the curve. The equation is given as

$$C = u\Delta t/\Delta x \leq Cmax \quad (13)$$

where C is the courant number, u is the dependent variable which is a magnitude of the velocity, Δt is the time interval and Δx is the space interval. The value of Cmax is typically 1 for the explicit methods. Eq. (13) is a one dimensional case of the CFL condition. The courant number can be enlarged by increasing the time interval or decreasing the space interval. The courant number controls the stability and it is necessary to choose the space and time intervals precisely.

- Evolve The Curve: We calculate the Sussman function [15] to maintain the smoothness of the curve. Re-initialization of the curve takes place and the process of Chan–Vese based segmentation continues until the liver is segmented completely and the curve cannot be evolved further.

3.2. GPU implementation of Chan–Vese

Our objective is a fast parallel implementation of the Chan–Vese approach for liver segmentation. In this section, we discuss the GPU implementation of the Chan–Vese approach. Chan–Vese is an iterative algorithm. The flow of GPU implementation of Chan–Vese approach for liver segmentation is shown in Fig. 2.

We load the liver image and send it to the GPU memory. The CPU calls the Chan–Vese kernel on the GPU. Each thread on the GPU in parallel performs the initialization of the curve. The stopping criteria is checked on the device memory to ensure the process is finished or not. If the process is finished then the control returns to the CPU storing the segmented image and the process stops.

Each thread in parallel is responsible for the calculation of the average value of the pixels inside and outside the curve. Inter block GPU synchronization (IBS) [36,37] between stages is essential and ensures valid data is communicated between the blocks. Then the Chan–Vese kernel on the GPU calculates the force based on the image pixels and the curvature and the gradient descent algorithm to minimize the energy given by Eq. (11). All the threads maintain the CFL condition for convergence and calculate the Sussman function to maintain the smoothness of the curve. The parallel threads reinitialize the curve and the process of liver segmentation using Chan–Vese continues until the curve cannot be evolved further. The process of segmentation stops and control returns to the CPU if the stopping criteria is satisfied.

These blocks communicate via IBS and the intermediate kernel calls are avoided using the proposed approach which helps to increase the performance. The kernel invokes enough blocks of threads to compute liver segmentation. The thread blocks on the GPU are the computational units launched in parallel to perform independent operations.

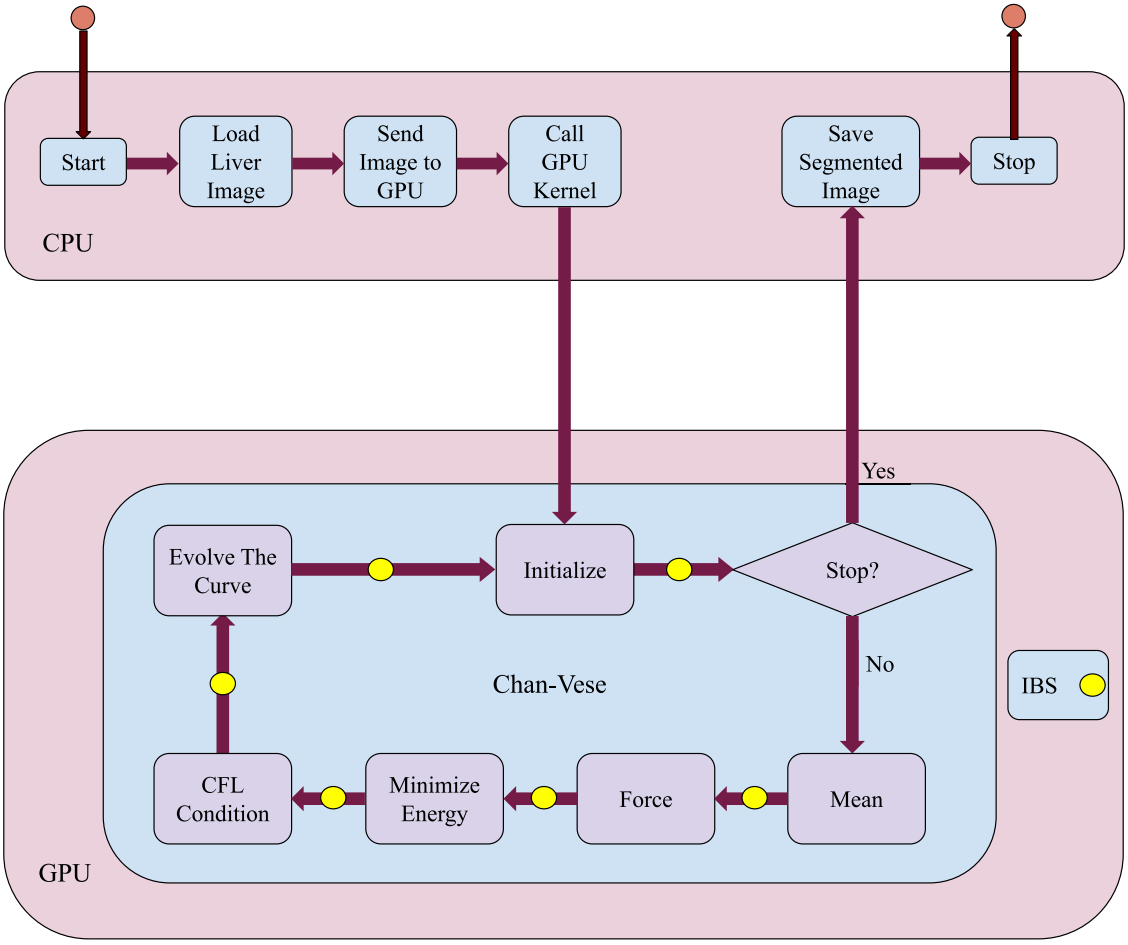

Fig. 2. GPU implementation of Chan–Vese.

The maximum number of active blocks are called persistent blocks [3,36]. However, the application may require more blocks compared to the persistent blocks. We apply a grid-stride loop so that the persistent blocks are iterated to perform the task of the remaining blocks [37,38].

Chan–Vese is a powerful approach for segmentation due to improved noise robustness although the quality of liver segmentation is questionable due to the low contrast of the liver images. Hence it is necessary to assess the impact of contrast enhancement on liver segmentation. We employ cross-modality guided liver contrast enhancement as a pre-processing step for liver segmentation. The parallel implementation of liver segmentation with contrast enhancement is discussed in the next section.

3.3. GPU implementation of Chan–Vese with enhancement

The Chan–Vese approach for liver segmentation results in false positives. In order to reduce the number of false positives and increase the sensitivity of liver segmentation, we enhance the CT liver image using cross-modality guided contrast enhancement. The flow of liver contrast enhancement and segmentation using Chan–Vese is shown in Fig. 3.

We load CT and MR images and send them to the GPU. The CPU invokes a single kernel on GPU for liver enhancement and segmentation. Liver enhancement improves the contrast of the CT liver image considering the MR image as the guidance image. The parallel computing units on the GPU match the histogram of the CT image with the guided MR image before performing segmentation. The liver contrast enhancement consists of the following modules:

- 2D Histogram: The contrast enhancement module calculates the 2D histogram of both CT and MR images. A 2D histogram is a plot of a pixels and neighboring pixels to discover the underlying 2D frequency distribution of the image. This involves calculating the frequency that how often the neighboring pair of values in an image occurs instead of just considering the individual pixel values [25,39,40].
- 2D Cumulative Distributive Function (CDF): The 2D histograms help to find the 2D CDFs of the CT and MR images for contrast enhancement. 2D CDF calculates the probability of a possible pixel pair in the CT and MR images [24,40].
- 2D Histogram Specification (HS): This is also called as histogram equalization. HS extends the most frequent intensity values improving the global contrast of the image [25,40].
- 2D Histogram Matching (HM): The process of histogram equalization over the CT image provides the enhanced image by mapping the modified intensity values obtained from the 2D histogram equalization to the corresponding pixels [24,25,39].

The enhanced CT image obtained from 2D cross-modality is sent to the Chan–Vese approach for segmentation. The GPU performs the segmentation and the control returns to the CPU saving the segmented liver image. This parallel Chan–Vese implementation is described in the previous Section 3.2.

4. Performance evaluation

In this section, we analyze and compare the performance of the Chan–Vese approach on CPU and GPU, the impact of enhancement

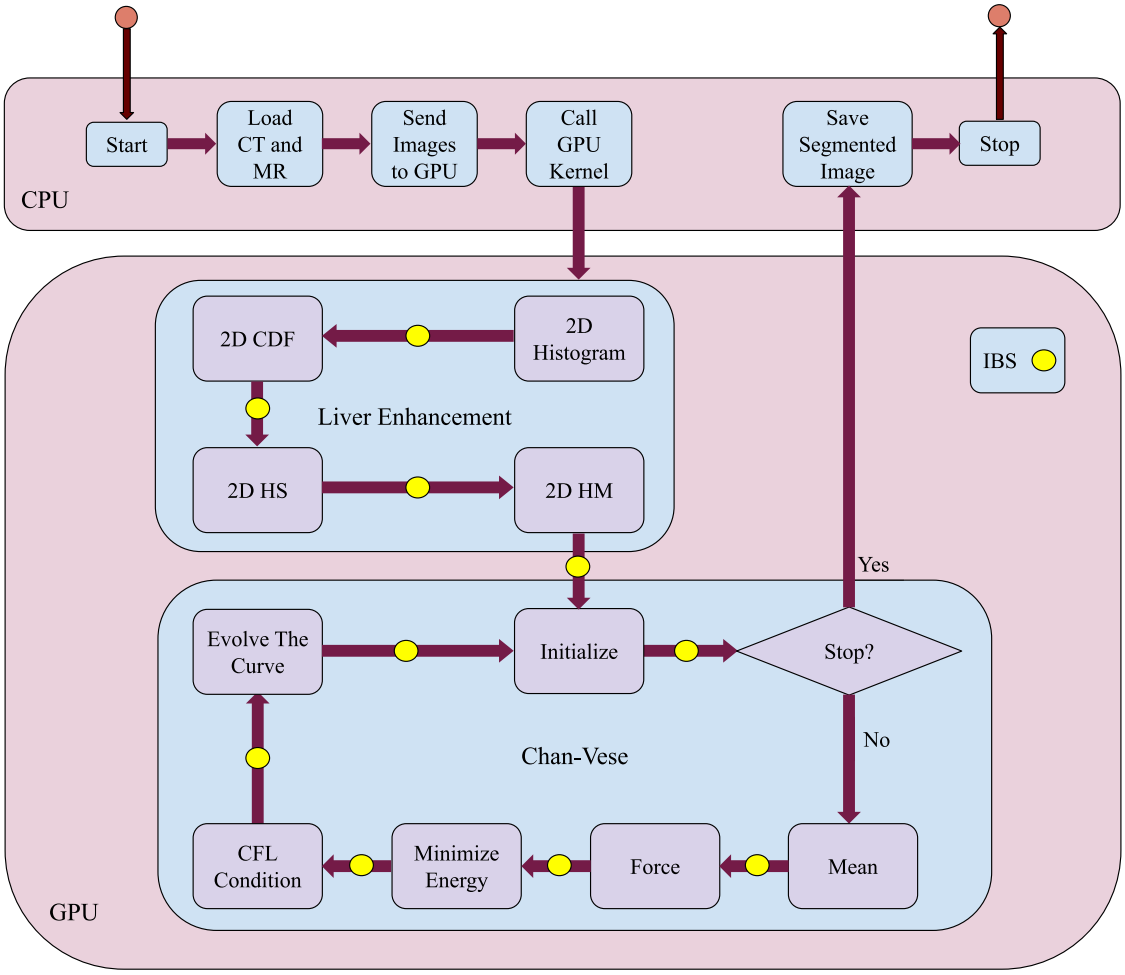

Fig. 3. GPU implementation of Chan–Vese with enhancement.

on liver segmentation and the quality of liver segmentation using dice score, sensitivity and accuracy. We use Intel(R) Core(TM) i7-7700HQ CPU @ 2.80 GHz RAM 24 GB, NVIDIA GPU GeForce GTX 1050 (RAM 4 GB) and CUDA Toolkit 10.1 for the implementation and we evaluate the performance of liver segmentation in the following section.

4.1. Dataset

Liver data for the research work has been acquired from The Intervention Centre, University of Oslo, Norway [3,41]. The ground truths for liver segmentation are provided by the clinician. Inter and intra observer errors exist while creating the ground truths for the input CT images. Intra observer error is when the same clinician creates the ground truth for the input CT image in different time stamps. Inter observer error is created when different clinicians create the ground truth for the same input CT image. Errors depend upon the registration of the input CT and MR images which are used for cross-modality guided contrast enhancement. Errors may also be introduced if clinicians use different registration techniques for the CT and MR slices. In this work, a 3D slicer is used for the registration.

The CT and MR volumes are loaded into the 3D Slicer and; then the region of interests (RoIs) are extracted from both volumes using the 'Surface Cut' and 'Mask Volume' options available in the 'Segment Editor' tool. The RoI can also be extracted using the 'Threshold' option in the 'Segment Editor'. The RoIs can be registered using 'General Registration' by selecting the appropriate Degree of Freedom) and 'Initialization Transform Mode'. Note that the registration results depend on the organs whose CT and MR volumes are being registered. Liver CT and MR images are quite challenging to register.

Table 1
Liver dataset.

Volume #	Total # of slices	Image size (wxh)	# of slices with Liver
28 059	59	462 × 321	6
23 186	87	405 × 346	6
18 152	139	512 × 512	5
10 504	59	460 × 306	7

Table 1 shows information about images of different sizes including the total number of liver slices used for the performance analysis from a particular volume. We validate the performance on 24 liver slices obtained from 4 different registered volumes. For ground truths, images are pre-processed through locally developed applications with a 3D Slicer. In some cases, the same application is used for liver segmentation and separation of portal and hepatic vessels although another possibility is to employ the active contour tool using ITK-SNAP and manual correction [41].

4.2. Quality of liver segmentation

We discuss the Chan–Vese approach for liver segmentation and the impact of cross-modality guided contrast enhancement on segmentation. The segmented results using Chan–Vese on the original and enhanced images are shown in Figs. 4, 5, and 6.

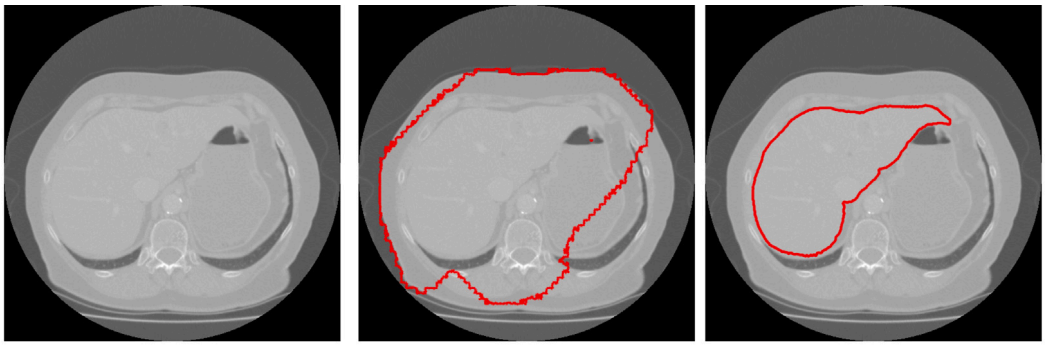

(a1) CT Image (a2) Seg (a3) GT

(a) Original Liver Image 1

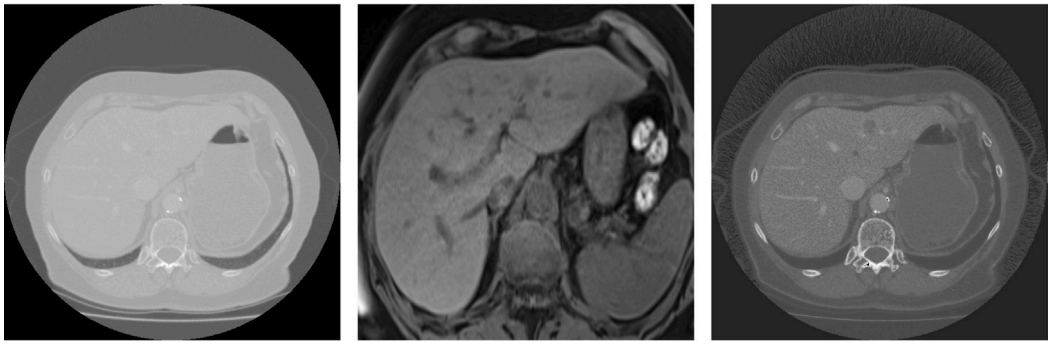

(b1) CT Image (b2) MR (b3) Enh_CT

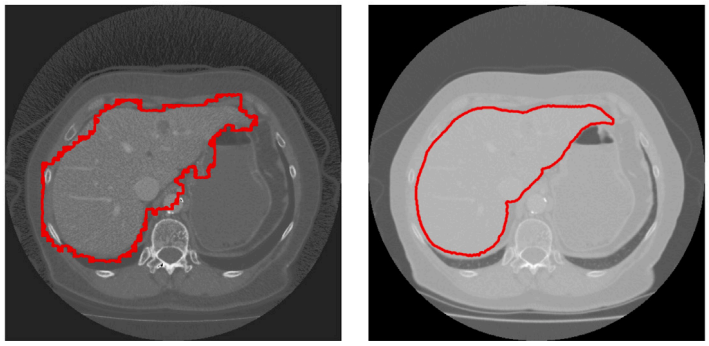

(b4) Seg (b5) GT

(b) Liver Enhancement and Segmentation from Enhanced CT Image 1

Fig. 4. Liver segmentation from original and enhanced CT image 1.

Table 2
Liver segmentation quality analysis.

Liver	Chan–Vese without enhancement			Chan–Vese with enhancement		
Slice #	Dice	Sensitivity	Accuracy	Dice	Sensitivity	Accuracy
1	0.504	0.831	0.719	0.904	0.979	0.969
2	0.533	0.669	0.748	0.895	0.961	0.966
3	0.762	0.882	0.896	0.894	0.988	0.967
4	0.759	0.868	0.890	0.879	0.991	0.961
5	0.721	0.829	0.858	0.815	0.901	0.917
Average	0.656	0.816	0.822	0.877	0.964	0.956
Std. Dev.	0.126	0.085	0.082	0.036	0.037	0.022

Figs. 4a, 5a, and 6a show the liver segmentation on original CT liver slices and Figs. 4b, 5b, and 6b show the liver segmentation with enhancement. We analyze the Chan–Vese based segmentation of the original and enhanced images. Figs. 4a2 and 4b4 show the Chan–Vese based liver segmentation of the original image (Fig. 4a1) and the enhanced image (Fig. 4b3) respectively and the ground truth is shown in Fig. 4a3 (or Figs. 4b5). Figs. 5a2 and 5b4 show liver segmentation from the original (Fig. 5a1) and enhanced image (Fig. 5b3) respectively with ground truth shown in Fig. 5a3 or 5b5. Similarly, Figs. 6a2 and 6b4 show liver segmentation from the original image (Fig. 6a1) and enhanced image (Fig. 6b3) respectively with ground truth shown in Fig. 6a3 or 6b5.

The input CT images and ground truths are the same for Figs. 4, 5, and 6. For example, the same input slices are shown in Figs. 4a1 and 4b1, 5a1 and 5b1, and 6a1 and 6b1. Identical ground truth images are shown in Figs. 4a3 and 4b5, 5a3 and 5b5, and 6a3 and 6b5. CT images (Figs. 4b1, 5b1, and 6b1) and MR images (Figs. 4b2, 5b2, and 6b2) are used to obtain the corresponding enhanced images (Figs. 4b3, 5b3 and 6b3) using cross-modality guided liver contrast enhancement. We compare the segmented result with the ground truth. It can be seen from the quality assessment of liver segmentation (Table 2) that the segmented liver is more accurate when the contrast of the liver is enhanced.

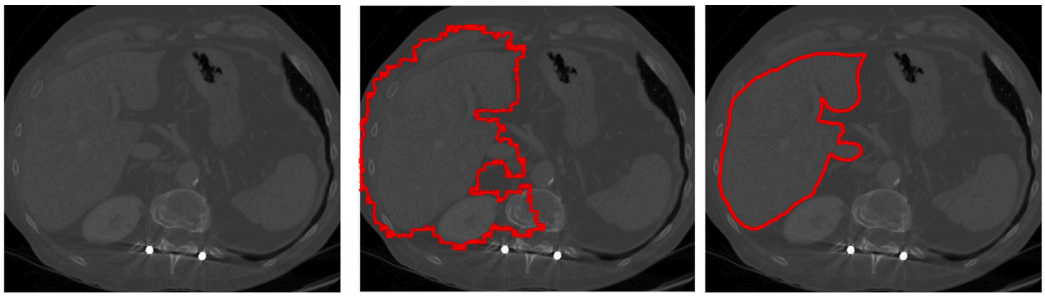

(a1) CT Image (a2) Seg (a3) GT

(a) Original Liver Image 2

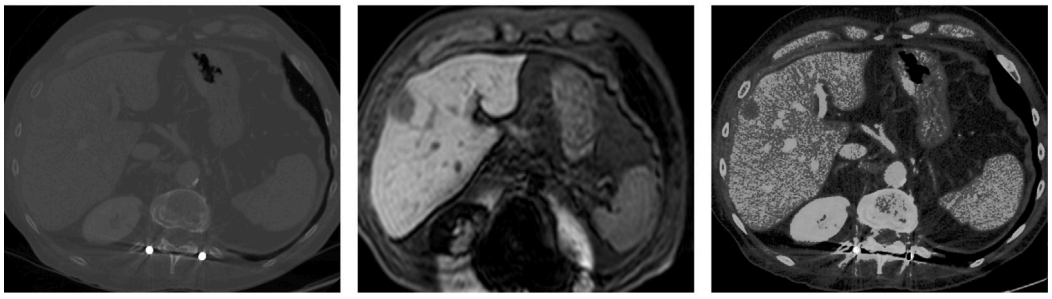

(b1) CT Image (b2) MR (b3) Enh_CT

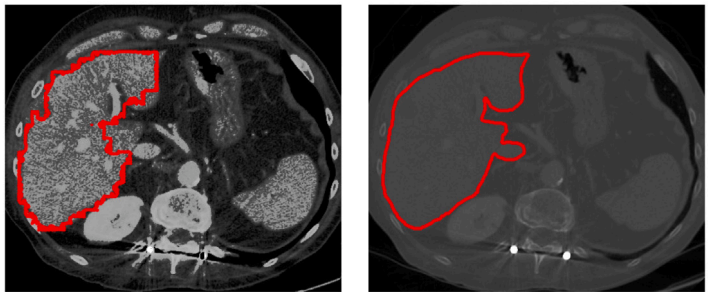

(b4) Seg (b5) GT

(b) Liver Enhancement and Segmentation from Enhanced CT Image 2

Fig. 5. Liver segmentation original and enhanced CT image 2.

Table 2 shows the quality assessment parameters i.e. dice, sensitivity and accuracy [22,23]. The dice measure indicates the region of overlap. Sensitivity also called the true positive rate defines whether the method is sensitive to the liver elements. Accuracy explains the number of liver and non-liver elements segmented accurately. It can be seen from Table 2 that the average dice, sensitivity and accuracy of the liver segmentation are 0.656 ± 0.126, 0.816 ± 0.085 and 0.822 ± 0.082 respectively on the original liver images and 0.877 ± 0.036, 0.964 ± 0.037 and 0.956 ± 0.022 respectively on the enhanced liver images. It can be seen that the Chan–Vese approach improves the dice, sensitivity and accuracy of liver segmentation on the enhanced liver slices.

We further analyze the performance of liver segmentation on 24 liver slices from 4 different volumes as shown in Fig. 7. Figs. 7a, 7b, 7c and 7d show the average values of accuracy, dice and sensitivity for the Chan–Vese approach both with and without enhancement. It can be seen from the performance results comparison (Figs. 7a, 7b, 7c and 7d) that the cross-modality guided liver enhancement improves the quality of segmentation in terms of accuracy, dice and sensitivity using the proposed Chan-Vese approach for liver segmentation.

A shape-intensity prior level set proposed by Wang et al. [35] used atlases which are weighted in the selected training datasets by calculating the similarities between the atlases and the test image to dynamically generate a subject-specific probabilistic atlas for the test image. The most likely liver region of the test image is further determined based on the generated atlas. A rough segmentation is obtained by a maximum a posteriori classification of the probability map, and the final liver segmentation is produced by a shape intensity prior level set in the most likely liver region. Thus the overall process is slow due to the training phase. The process also depends upon large datasets for training.

In the proposed work, we do not use training and hence do not need large datasets. In the absence of strong edges, region based formulation using Chan–Vese performs well for segmentation which can be seen from the performance results and the authors employ a cross-modality guided image enhancement as a pre-processing step which further improves the quality of segmentation. The proposed segmentation algorithm can delineate liver boundaries that have levels of variability similar to those obtained manually. The proposed approach speeds up the overall process of liver segmentation by 100 times on the GPU compared to the CPU implementation.

MICCAI test data provided by the organizers of the "SLIVER07" contains clinical 3D computed tomography (CT) scans [42,43]. The proposed method is based on a cross-modality approach in which we

(a1) CT Image (a2) Seg (a3) GT

(a) Original Liver Image 3

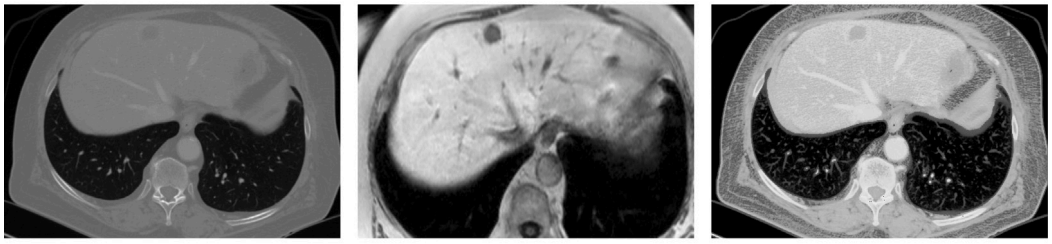

(b1) CT Image (b2) MR (b3) Enh_CT

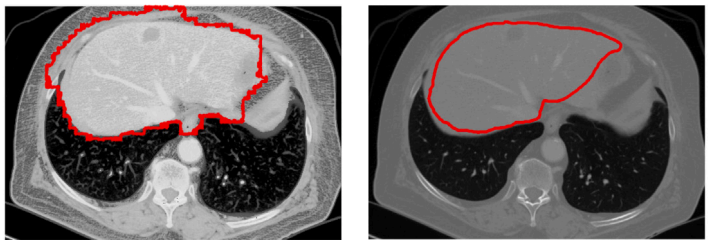

(b4) Seg (b5) GT

(b) Liver Enhancement and Segmentation from Enhanced CT Image 3

Fig. 6. Liver segmentation from original and enhanced CT image 3.

require MR scans for the guided enhancement. To the best of our knowledge, this is the first non-learning approach using cross-modality guided contrast enhancement for liver segmentation. The registered MR image is used to enhance the low quality CT image. This is done by using a non-learning approach of 2D histogram equalization and matching.

Kavur et al. [44] reported that CT-MR liver segmentation is inferior to CT or MR image segmentation due to CT-MR visual difference. The study from CHAOS Challenge by Kavur et al. [44], proposes a learning based approach for segmentation taking CT-MR images as training inputs in order to increase the training data and reveal common features of incorporated modalities for an organ. The deep model learns from the combined CT and MR datasets. The cross-modality (CT-MR) learning proved to be more challenging than individual training. Such complicated tasks could benefit from spatial priors, global topological, or shape-representations in their loss functions as employed by some of the deep learning models.

However, we show that the enhanced CT image using cross-modality approach provides better segmentation results in terms of dice, accuracy and sensitivity compared to the original CT image. In the next section, we discuss the speedup obtained by the proposed GPU implementation in comparison to the CPU.

4.3. Speedup

In this section, we discuss the speedup obtained by the GPU implementation of Chan–Vese compared to CPU implementation and analyze the impact of enhancement on speedup. The speedup analysis of liver segmentation on the CPU and the GPU is shown in Table 3.

Table 3
Liver segmentation speedup analysis.

Liver	Chan–Vese without enhancement			Chan–Vese with enhancement		
Slice #	CPU (s)	GPU (s)	Speedup	CPU (s)	GPU (s)	Speedup
1	4.324	0.276	15.667	276.15	2.78	99.335
2	4.117	0.256	16.082	270.098	2.44	110.696
3	2.679	0.195	13.738	173.93	1.95	89.195
4	2.857	0.211	13.54	165.03	1.65	100.018
5	3.112	0.219	14.21	175.82	1.73	101.63
Average	3.49425	0.2345	14.647	221.302	2.205	99.811
Std. Dev.	0.752	0.033	1.155	55.8	0.484	7.65

The computational complexity of the proposed Chan–Vese algorithm is O(N) where N is the number of elements in the CT image. So even for the large images, it is also very efficient. The average time taken by CPU implementations (with and without enhancement) are 221.302 ± 55.8 s and 3.49425 ± 0.752 s respectively and GPU implementations are 2.205 ± 0.484 s and 0.2345 ± 0.033 s respectively. Hence the GPU implementations (with and without enhancement) on an NVIDIA GPU GeForce GTX 1050 with RAM 4 GB provide an average speedup of 99.811 ± 7.65 times and 14.647 ± 1.155 times in comparison to the CPU implementation on Intel(R) Core(TM) i7-7700HQ CPU @ 2.80 GHz RAM 24 GB. The reason behind the obtained speedup is the

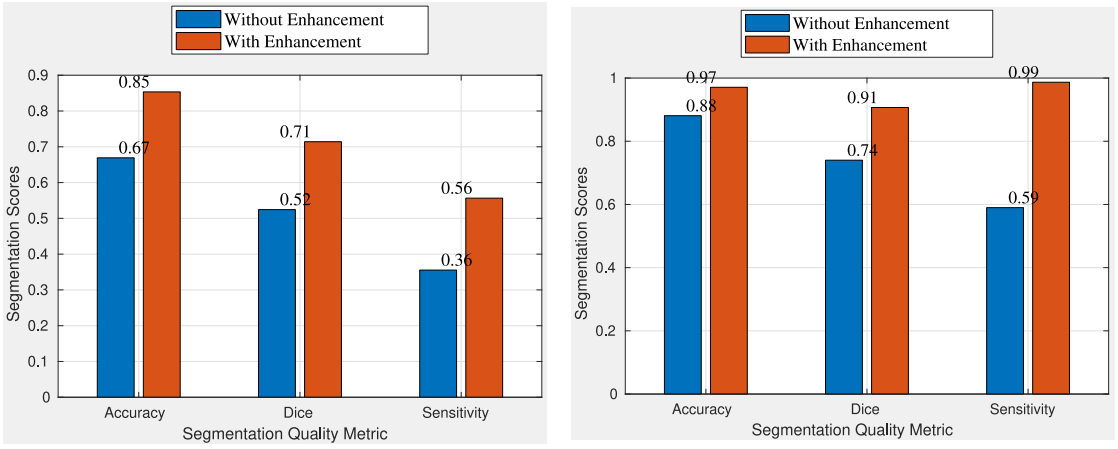

(a) Volume 28059

(b) Volume 23186

(c) Volume 18152

(d) Volume 10504

Fig. 7. Segmentation quality assessment on different volumes.

avoidance of intermediate kernel calls and exploiting high level parallelism present in liver contrast enhancement and Chan–Vese approach for image segmentation.

Liver contrast enhancement uses a 2D histogram technique which includes histogram of the pair of neighboring elements in the CT and MR images. Hence the complexity increases due to pairwise histogram analysis of cumulative distributive function and histogram matching. The Chan–Vese approach includes time-consuming numerical calculations of partial differential equations. These tasks i.e. 2D histogram calculations and solutions to the partial differential equations have been implemented on an NVIDIA GPU in parallel for liver segmentation providing an average speedup of 99.811 ± 7.65 compared to the CPU implementation. The time is computed in GPU time and it is optimized by avoiding the intermediate memory transfers.

We perform the statistical treatment of results. P value from analysis of variance (ANOVA) for the datasets is $2.43 * 10^{-14}$ which is less than 0.0005 (0.05%). We reject the null hypothesis and conclude that not all means are equal which confirms the means are statistically significant for the experiments.

4.4. Discussion

The Chan–Vese algorithm is quite slow due to time-consuming computations of the partial differential equations, especially when dealing with large medical datasets. It can pose a problem for a real-time implementation and an efficient parallel approach is highly desirable. The Chan–Vese algorithm is a very powerful algorithm due to improved noise robustness. However, there are cases in which the liver segmentation is less accurate and sensitive. It is necessary to enhance the contrast of the liver for more accurate segmentation. Hence, we incorporate cross-modality guided image enhancement as a pre-processing step to improve the quality of liver segmentation. However, the cross-modality approach includes 2D histogram analysis which is time-consuming and includes repetitive tasks of pairwise histogram analysis of liver image elements. This is also applicable to numerical calculations of the partial differential equations in Chan–Vese. These repetitive tasks are implemented on an NVIDIA GPU using threads of blocks and the performance is improved significantly in comparison to the CPU implementation.

5. Conclusion

In this paper, we propose a fast parallel liver segmentation using the Chan–Vese approach and study the impact of contrast enhancement on liver segmentation. The proposed approach is fast, accurate and outperforms other approaches for low quality CT liver slices. The proposed segmentation algorithm can delineate liver boundaries that have levels of variability similar to those obtained manually. GPU implementation of the proposed approach speeds up the overall process of liver segmentation by 100 times compared to the CPU implementation.

Chan–Vese approach for liver segmentation is less sensitive (0.816 ± 0.085 from Table 2) when applied to original CT liver images. Sensitivity should be increased for more accurate liver segmentation. Hence, we apply a cross-modality guided contrast enhancement on CT liver images and segment the liver using the proposed Chan–Vese approach for segmentation. The work compares CPU and GPU implementations with and without enhancement. The average dice, sensitivity and accuracy of the liver segmentation are 0.877 ± 0.036, 0.964 ± 0.037 and 0.956 ± 0.022 respectively on the enhanced liver images. The cross-modality guided contrast enhancement improves the quality of the results by decreasing the false positives. The proposed GPU implementation with enhancement improves the speedup by 99.811 ± 7.65 times over CPU implementation. Hence the parallel implementation of Chan–Vese approach for liver segmentation is faster when implemented on the GPU and more accurate when the contrast of the CT liver image is enhanced.

Declaration of competing interest

The authors declare that they have no known competing financial interests or personal relationships that could have appeared to influence the work reported in this paper.

Acknowledgments

The work is supported by the project High Performance soft tissue Navigation (HiPerNav). This project has received funding from the European Union Horizon 2020 research and innovation program under grant agreement No. 722068. We thank The Intervention Centre, Oslo University Hospital, Oslo, Norway for providing the CT images with ground truths for the clinical validation of the liver segmentation.

References

[1] M.F. Hashmi, S. Katiyar, A.G. Keskar, N.D. Bokde, Z.W. Geem, Efficient pneumonia detection in chest xray images using deep transfer learning, Diagnostics 10 (6) (2020) http://dx.doi.org/10.3390/diagnostics10060417.

[2] K.K. Delibasis, A. Kechriniotis, I. Maglogiannis, A novel tool for segmenting 3D medical images based on generalized cylinders and active surfaces, Comput. Methods Programs Biomed. 111 (1) (2013) 148–165, http://dx.doi.org/10.1016/j.cmpb.2013.03.009.

[3] N. Satpute, R. Naseem, R. Palomar, O. Zachariadis, J. Gómez-Luna, F.A. Cheikh, J. Olivares, Fast parallel vessel segmentation, Comput. Methods Programs Biomed. 192 (2020) 105430, http://dx.doi.org/10.1016/j.cmpb.2020.105430.

[4] S.K. Siri, M.V. Latte, Combined endeavor of neutrosophic set and Chan-Vese model to extract accurate liver image from CT scan, Comput. Methods Programs Biomed. 151 (2017) 101–109.

[5] A.P. Rao, N. Bokde, S. Sinha, Photoacoustic imaging for management of breast cancer: A literature review and future perspectives, Appl. Sci. 10 (3) (2020) 767.

[6] R. Palomar, J. Gómez-Luna, F.A. Cheikh, J. Olivares-Bueno, O.J. Elle, High-performance computation of bézier surfaces on parallel and heterogeneous platforms, Int. J. Parallel Program. 46 (6) (2018) 1035–1062.

[7] O. Zachariadis, A. Teatini, N. Satpute, J. Gómez-Luna, O. Mutlu, O.J. Elle, J. Olivares, Accelerating B-spline interpolation on GPUs: Application to medical image registration, Comput. Methods Programs Biomed. 193 (2020) 105431, http://dx.doi.org/10.1016/j.cmpb.2020.105431.

[8] E. Smistad, T.L. Falch, M. Bozorgi, A.C. Elster, F. Lindseth, Medical image segmentation on GPUs–A comprehensive review, Med. Image Anal. 20 (1) (2015) 1–18.

[9] E. Smistad, M. Bozorgi, F. Lindseth, FAST: framework for heterogeneous medical image computing and visualization, Int. J. Comput. Assist. Radiol. Surg. 10 (11) (2015) 1811–1822.

[10] R. Hemalatha, T. Thamizhvani, A.J.A. Dhivya, J.E. Joseph, B. Babu, R. Chandrasekaran, Active contour based segmentation techniques for medical image analysis, Med. Biol. Image Anal. (2018) 17.

[11] X. Lu, Q. Xie, Y. Zha, D. Wang, Fully automatic liver segmentation combining multi-dimensional graph cut with shape information in 3D CT images, Sci. Rep. 8 (1) (2018) 10700.

[12] X.-F. Wang, D.-S. Huang, H. Xu, An efficient local Chan–Vese model for image segmentation, Pattern Recognit. 43 (3) (2010) 603–618.

[13] S. Tomoshige, E. Oost, A. Shimizu, H. Watanabe, S. Nawano, A conditional statistical shape model with integrated error estimation of the conditions; Application to liver segmentation in non-contrast CT images, Med. Image Anal. 18 (1) (2014) 130–143, http://dx.doi.org/10.1016/j.media.2013.10.003.

[14] J. Duan, Z. Pan, X. Yin, W. Wei, G. Wang, Some fast projection methods based on Chan-Vese model for image segmentation, EURASIP J. Image Video Process. 2014 (1) (2014) 7, http://dx.doi.org/10.1186/1687-5281-2014-7.

[15] W. Aydi, N. Masmoudi, L. Kamoun, Active contour without edges vs GVF active contour for accurate pupil segmentation, Int. J. Comput. Appl. 54 (4) (2012) Citeseer.

[16] R. Cohen, The chan-vese algorithm, 2011, CoRR abs/1107.2782. arXiv:1107.2782. URL http://arxiv.org/abs/1107.2782.

[17] A. Hoogi, C.F. Beaulieu, G.M. Cunha, E. Heba, C.B. Sirlin, S. Napel, D.L. Rubin, Adaptive local window for level set segmentation of CT and MRI liver lesions, Med. Image Anal. 37 (2017) 46–55, http://dx.doi.org/10.1016/j.media.2017.01.002.

[18] D. Smeets, D. Loeckx, B. Stijnen, B.D. Dobbelaer, D. Vandermeulen, P. Suetens, Semi-automatic level set segmentation of liver tumors combining a spiral-scanning technique with supervised fuzzy pixel classification, Med. Image Anal. 14 (1) (2010) 13–20, http://dx.doi.org/10.1016/j.media.2009.09.002.

[19] L. He, S. Osher, Solving the Chan-Vese model by a multiphase level set algorithm based on the topological derivative, in: International Conference on Scale Space and Variational Methods in Computer Vision, Springer, 2007, pp. 777–788.

[20] K. Zhang, H. Song, L. Zhang, Active contours driven by local image fitting energy, Pattern Recognit. 43 (4) (2010) 1199–1206.

[21] E. Smistad, A.C. Elster, F. Lindseth, GPU accelerated segmentation and centerline extraction of tubular structures from medical images, Int. J. Comput. Assist. Radiol. Surg. 9 (4) (2014) 561–575.

[22] Z. Yan, X. Yang, K. Cheng, A three-stage deep learning model for accurate retinal vessel segmentation, IEEE J. Biomed. Health Inf. 23 (4) (2019) 1427–1436, http://dx.doi.org/10.1109/JBHI.2018.2872813.

[23] M.H. Yap, G. Pons, J. Martí, S. Ganau, M. Sentís, R. Zwiggelaar, A.K. Davison, R. Martí, Automated breast ultrasound lesions detection using convolutional neural networks, IEEE J. Biomed. Health Inf. 22 (4) (2018) 1218–1226, http://dx.doi.org/10.1109/JBHI.2017.2731873.

[24] T. Celik, Two-dimensional histogram equalization and contrast enhancement, Pattern Recognit. 45 (10) (2012) 3810–3824, http://dx.doi.org/10.1016/j.patcog.2012.03.019.

[25] S.-W. Jung, Two-dimensional histogram specification using two-dimensional cumulative distribution function, Electron. Lett. 50 (12) (2014) 872–874.

[26] T. Kronfeld, D. Brunner, G. Brunnett, Snake-based segmentation of teeth from virtual dental casts, Comput.-Aided Des. Appl. 7 (2) (2010) 221–233.

[27] S. Roy, S. Mukhopadhyay, M.K. Mishra, Enhancement of morphological snake based segmentation by imparting image attachment through scale-space continuity, Pattern Recognit. 48 (7) (2015) 2254–2268.

[28] Y. Cheng, X. Hu, J. Wang, Y. Wang, S. Tamura, Accurate vessel segmentation with constrained b-snake, IEEE Trans. Image Process.: Publ. IEEE Signal Process. Soc. 24 (2015) http://dx.doi.org/10.1109/TIP.2015.2417683.

[29] A. Khadidos, V. Sanchez, C. Li, Active contours based on weighted gradient vector flow and balloon forces for medical image segmentation, in: 2014 IEEE International Conference on Image Processing (ICIP), 2014, pp. 902–906, http://dx.doi.org/10.1109/ICIP.2014.7025181.

[30] Z.-B. Li, X.-Z. Xu, Y. Le, F.-Q. Xu, An improved balloon snake for HIFU image-guided system, J. Med. Ultrason. 41 (3) (2014) 291–300.

[31] E. Smistad, A.C. Elster, F. Lindseth, Real-time gradient vector flow on GPUs using OpenCL, J. Real-Time Image Process. 10 (1) (2015) 67–74.

[32] H. Zhou, X. Li, G. Schaefer, M.E. Celebi, P. Miller, Mean shift based gradient vector flow for image segmentation, Comput. Vis. Image Underst. 117 (9) (2013) 1004–1016.

[33] B. Chen, J. Zhao, E. Dong, J. Chen, Y. Zhao, Z. Yuan, An improved GVF snake model using magnetostatic theory, in: Computer, Informatics, Cybernetics and Applications, Springer, 2012, pp. 431–440.

[34] J. Zhao, B. Chen, M. Sun, W. Jia, Z. Yuan, Improved algorithm for gradient vector flow based active contour model using global and local information, Sci. World J. 2013 (2013).

[35] J. Wang, Y. Cheng, C. Guo, Y. Wang, S. Tamura, Shape–intensity prior level set combining probabilistic atlas and probability map constrains for automatic liver segmentation from abdominal ct images, Int. J. Comput. Assist. Radiol. Surg. 11 (2015) http://dx.doi.org/10.1007/s11548-015-1332-9.

[36] K. Gupta, J.A. Stuart, J.D. Owens, A study of persistent threads style GPU programming for GPGPU workloads, in: Innovative Parallel Computing-Foundations & Applications of GPU, Manycore, and Heterogeneous Systems (INPAR 2012), IEEE, 2012, pp. 1–14.

[37] M. Sourouri, S.B. Baden, X. Cai, Panda: A compiler framework for concurrent CPU+GPU execution of 3D stencil computations on GPU-accelerated supercomputers, Int. J. Parallel Program. 45 (3) (2017) 711–729.

[38] M. Harris, CUDA Pro Tip:Write Flexible Kernels with Grid-Stride Loops, GitHub, 2015, URL http://goo.gl/b8Vmkh.

[39] N. Satpute, R. Naseem, E. Pelanis, J. Gomez-Luna, F. Alaya Cheikh, O.J. Elle, J. Olivares, GPU acceleration of liver enhancement for tumor segmentation, Comput. Methods Programs Biomed. 184 (2020) 105285, http://dx.doi.org/10.1016/j.cmpb.2019.105285.

[40] R. Naseem, F.A. Cheikh, A. Beghdadi, O.J. Elle, F. Lindseth, Cross modality guided liver image enhancement of CT using MRI, in: 2019 8th European Workshop on Visual Information Processing (EUVIP), IEEE, 2019, pp. 46–51.

[41] Å.A. Fretland, V.J. Dagenborg, G.M.W. Bjørnelv, A.M. Kazaryan, R. Kristiansen, M.W. Fagerland, J. Hausken, T.I. Tønnessen, A. Abildgaard, L. Barkhatov, et al., Laparoscopic versus open resection for colorectal liver metastases, Ann. Surg. 267 (2) (2018) 199–207.
[42] C. Shi, Y. Cheng, F. Liu, Y. Wang, J. Bai, S. Tamura, A hierarchical local region-based sparse shape composition for liver segmentation in CT scans, Pattern Recognit. 50 (2016) 88–106.
[43] C. Shi, Y. Cheng, J. Wang, Y. Wang, K. Mori, S. Tamura, Low-rank and sparse decomposition based shape model and probabilistic atlas for automatic pathological organ segmentation, Med. Image Anal. 38 (2017) 30–49.
[44] A.E. Kavur, N.S. Gezer, M. Barış, P.-H. Conze, V. Groza, D.D. Pham, S. Chatterjee, P. Ernst, S. Özkan, B. Baydar, et al., CHAOS challenge–combined (CT-MR) healthy abdominal organ segmentation, 2020, arXiv preprint arXiv:2001.06535.

Nitin Satpute is a researcher and PhD candidate at University of Cordoba. He works on GPU acceleration for medical image enhancement and segmentation algorithms as a part of HiPerNav EU project. In 2018, he worked on liver segmentation at OUH, Oslo, Norway. In 2019, he worked on liver enhancement at NTNU Gjovik Norway, where he developed fast parallel cross modality approach for liver contrast enhancement. He holds Master of Engineering in Embedded Systems from BITS Pilani, India. His research interests include GPU computing, Medical Imaging, Re-configurable Computing and Video Processing.

Juan Gómez-Luna is a postdoctoral researcher at ETH Zürich. He received the BS and MS degrees in Telecommunication Engineering from the University of Sevilla, Spain, in 2001, and the PhD degree in Computer Science from the University of Córdoba, Spain, in 2012. Between 2005 and 2017, he was a lecturer at the University of Córdoba. His research interests focus on Processing-in-Memory, GPUs and heterogeneous systems, medical imaging, and bioinformatics.

Joaquín Olivares was born in Elche, Spain. He received the B.S. and M.S. degree in Computer Sciences in 1997, and 1999, respectively, and the M.S. degree in Electronics Engineering in 2003, all from the Universidad de Granada, Spain. He received the Ph.D. degree in 2008 at the Universidad de Cordoba, Spain. He is Associate Professor with the Electronic and Computer Engineering Department at the Universidad de Cordoba, Spain, since 2001. He is founder and head of the Advanced Informatics Research Group. His research interests are in the field of embedded systems, computer vision, and high performance computing.